Achieving high precision photometry for transiting exoplanets with a low cost robotic DSLR-based imaging system

Olivier Guyon*[a,b], Frantz Martinache[a]
[a]Subaru Telescope, National Astronomical Observatory of Japan, 650 N. A'ohoku Place, Hilo, HI 96720, USA;
[b]Steward Observatory, University of Arizona, 933 N. Cherry Ave, Tucson, AZ 85721, USA

ABSTRACT

We describe a low cost high precision photometric imaging system, which has been in robotic operation for one and half year on the Mauna Loa observatory (Hawaii). The system, which can be easily duplicated, is composed of commercially available components, offers a 150 sq deg field with two 70mm entrance apertures, and 6-band simultaneous photometry at a 0.01 Hz sampling. The detectors are low-cost commercial 3-color CMOS array, which we show is an attractive cost-effective choice for high precision transit photometry. We describe the design of the system and show early results.

A new data processing technique was developed to overcome pixelization and color errors. We show that this technique, which can also be applied on non-color imaging systems, essentially removes pixelization errors in the photometric signal, and we demonstrate on-sky photometric precision approaching fundamental error sources (photon noise and atmospheric scintillation). We conclude that our approach is ideally suited for exoplanet transit survey with multiple units. We show that in this scenario, the success metric is purely cost per etendue, which is at less than $10000s per square meter square degree for our system.

Keywords: Exoplanet transit, photometry

1. INTRODUCTION

We describe a small experimental low-cost robotic wide field imaging system for astronomy and atmospheric science based on low-cost digital single lens reflex (DSLR) camera with CMOS detectors[1-6]. The project is a collaboration with the VYSOS project[7], and is located at the Mauna Loa Observatory, an excellent site for nighttime astronomy.

This project is aimed at exploring a low-cost approach to perform a scientifically useful all-sky 3-color imaging survey. The system was installed on Mauna Loa observatory in December 2010, and started fully robotic operation in early 2011 with a single camera. It was upgraded to a 2-camera system in summer 2011. The first year of observations (until summer 2012) was used to evaluate scientific performance and system reliability, as well as develop data reduction algorithms which will process the large volume of data acquired. This project focuses especially on:

- Low surface brightness observations of the night sky, large size features (atmospheric and astronomical)
- High precision photometry in 3 colors simultaneously (variable stars, exoplanet transits)

All hardware and software for the system are open source, and is meant to help other amateur and professional astronomers duplicate and improve this approach. The low cost of the system, its ability to produce well calibrated 3-color photometry (under study) and ease of making color images make this system suitable for both astronomical research and outreach.

*guyon@naoj.org; phone 1 818 293-8826

2. SYSTEM OVERVIEW

2.1 Introduction

Figure 1. Left: Image of the robotic camera system on Mauna Loa observatory. Mauna Kea, to the North, can be seen in the background on the left. The cameras are mounted on an equatorial motorized mount on top of a metallic frame. The domes on the right host the VYSOS project robotic telescopes. Right: View pointing South. The Mauna Loa solar observatory is in the background. Openings for the two objectives can be seen on the front of the cameras enclosure. Note that the system does not have a dome, and simply points down during daytime or bad weather. The small shiny box on the right of the camera system is hosting humidity, temperature and cloud sensors.

The imaging system consists of two commercial digital cameras: models Canon 500D and 550D. The Canon 500D native IR-blocking filter in front of the sensor was replaced with a filter offering higher transmission in the red. The 550D is unmodified and includes the native IR-blocking filter. The two cameras combination therefore offers six different colors. Each camera is equipped with a 85mm focal length lens at F1.2 (Canon EF 85mm f/1.2L II USM). The cameras are pointed at the same direction, and mounted on a 2-axis equatorial mount (Orion Atlas EQ-G). The system (camera + mount) is computer controlled with a laptop. The data is stored on the laptop hard drive, and copied to an external hard drive. The main system characteristics are listed in table 1.

Table 1. Imaging system characteristics.

	Camera 1	**Camera 2**
Camera body	Canon 500D	Canon 550D
field of view	150 sq deg (10x15 deg)	
Aperture	85mm F1.2 lens (70mm diam)	
Pixel size	10”	8”
Detector	CMOS color, 15 Mpix	CMOS color, 18 Mpix
Sensitivity	photon noise limited on background, mV~15.5 point source sensitivity in 4mn	

The data volume is approximately 5 GB per night, stored locally. The data is physically retrieved every ~2 month by copying it to an external drive (2 month of data = 300 GB). The average total power consumption is about 25W (including approximately 10W for laptop) at night, and 15W during the day.

2.2 Detector and sensitivity

In this section, we report the results of calibration and performance measurement for the Canon 500D camera body (camera #1 of the system), with a 15Mpix CMOS sensor. Detector characteristics were measured and used to derive the system sensitivity and optimal photon-noise limited exposure times and ISO setting.

The **detector noise** was measured by differencing two short exposure dark frames at 800 ISO. The RMS deviation between the two images is divided by sqrt(2) to compute the readout noise. The **Gain** was measured by differencing two images taken with a background level of ~1200 ADU (after subtracting bias), using green pixels only. A quadratic subtraction of readout noise is performed to isolate and measure photon noise. Scaling to other ISO values is done assuming linearly of gain with ISO setting.

Table 2. Information on video and audio files that can accompany a manuscript submission.

	ISO 100	**ISO 200**	**ISO 400**	**ISO 800**	**ISO 1600**
Readout noise [ADU]	10.9	11.6	13.94	19.87	32.27
Gain [e-/ADU]	1.36	0.68	0.34	0.17	0.09
Readout noise [e-]	15.8	7.91	4.74	3.38	2.74
(RON=photon noise) level [ADU]	161.5	92.08	66.11	67.16	88.49
Minimum exposure time (no Moon)	190.0 s	54.2 s	19.4 s	9.9 s	6.5 s
Number of exposures per hr	18.95	66.4	185.6	363.6	553.8
Saturation level [e-/frame]	22282.2	11141.1	5570.6	2785.3	1392.6
Saturation level [e-/hr]	4.22E+005	7.40E+005	1.03E+006	1.01E+006	7.71E+005
Dynamical range for 1 hr	6542	11471	16026	15702	11951

Measurement results are shown in table 2. The 4th entry of the table shows the count level for which readout noise is equal to photon noise. Exposures should be sufficiently long to ensure that the background counts are above this level to ensure photon-noise limited performance.

The sky background level was measured under dark sky (no moon), with the 85mm lens at F1.2 and ISO 800 setting. Values are given below for each of the 3 color channels.

- RED pixels: 8.9 cnt / sec / pix @ 800 ISO = 1.513 e- / sec / pix
- GREEN pixels: 11.1 cnt / sec / pix @ 800 ISO = 1.887 e- / sec / pix
- BLUE pixels: 6.8 cnt / sec / pix @ 800 ISO = 1.156 e- / sec / pix

The blue pixels have the smallest counts. The minimum exposure times to ensure photon-noise limited performance are given by combining the sky background count levels with the previously derived minimum count level to ensure photon-noise limited sensitivity. Table 2 shows that under dark conditions, this exposure time ranges from 6.5 sec at ISO 1600 to 190 sec at ISO 100.

The dynamical range is the ratio between noise and saturation for a single pixel. All values given for a 1hr observation, assuming that the exposure time is chosen such that readout noise = sky background photon noise under dark conditions, and that readout time is much less than exposure time.

The best dynamical range is achieved by co-adding exposures taken at ISO 400 or ISO 800, with individual exposures of approximately 20 sec (@ ISO 400) and 10 sec (@ ISO 800). In practice, this optimal exposure time cannot be sustained for a long survey: at 20 sec per exposure, 10 hr observation per night, the shutter lifetime (rated at 90000 exposures) corresponds to 50 nights of observation. **Single frame exposure time is therefore a compromise between shutter lifetime and dynamical range** . The imaging system currently operates at ISO 100 with exposure times longer than 200 sec in dark time to optimize shutter lifetime, and operation without shutter is being explored. At ISO100, 120sec, saturation is reached on the best frames for mV~10.5 (approximate).

2.3 Optics and image quality

The system is acquiring images at F1.2 (lens fully open) to maximize sensitivity. Image quality is good through the field, with PSF FWHM of 1.5 to 2 pixel. Figure 2 shows a sample image: the PSF degradation at the edge of the field is noticeable but moderate (FWHM ~ 2pix).

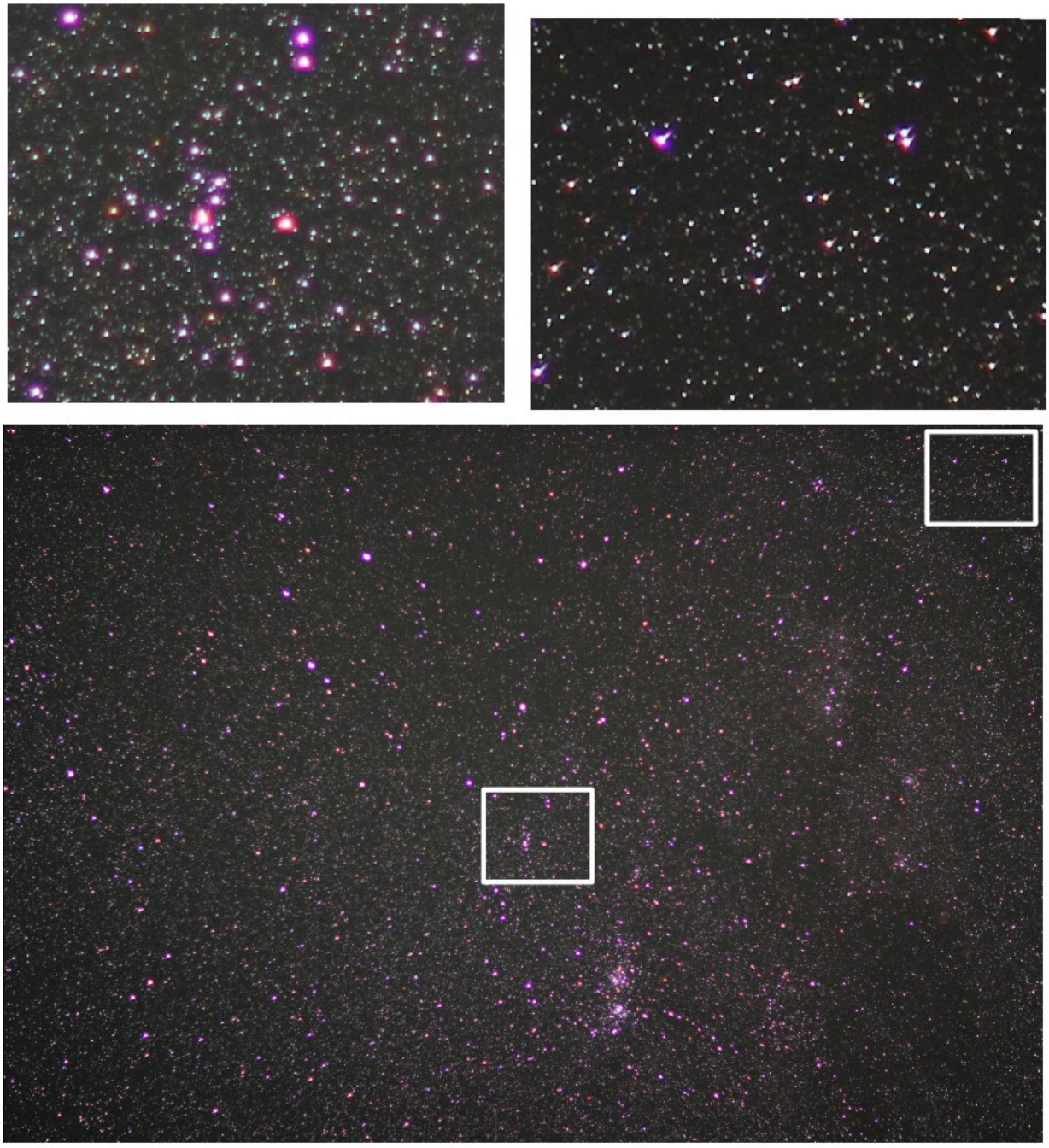

Figure 2. Sample image from camera #2 (287 sec exposure at ISO 100). The full field image (10x15 deg) is shown in the bottom. Details of the central and corner regions are shown at the top.

3. HARDWARE IMPLEMENTATION

3.1 Weatherproofing

The durability of the system is a strong requirement. In order to keep the system simple and low cost, it does not have a dome: the camera points down when it rains/snows or when there are clouds. The system includes several sensors to determine if the weather is suitable for observing:

- Four webcams acquire images every minute, and are used to automatically confirm nighttime (which is primarily derived from the Sun altitude below the horizon, according to the computer clock). Visual inspection of the webcam images can also identify snow/ice on the mount or camera.
- Temperature probes facing the sky and the ground are used to detect clear sky at night: if the sky is clear, the upward looking temperature probe is colder than the downward looking probe (thermal radiation to the sky). If this temperature difference is larger than a preset limit, then the sky is deemed clear and observing can start.
- A humidity sensor

In addition to these sensors, the weather information provided by the VYSOS observatory and the the Mauna Loa observatory are downloaded every minute from the network. Decision to observe is made from all sensor values.

The system is designed to minimize the long-term impact of weather :

- no exposed plastic (to avoid UV degradation of plastics)
- mount has been sealed against water with silicone
- camera is sealed (cover) except at the front (lens) which points down when weather is bad
- use of weather-resistant materials when possible: Aluminum instead of steel when possible, Stainless instead of standard steel for bolts/nuts, use of Kapton tape when tape must be exposed.

3.2 Mount and Tracking

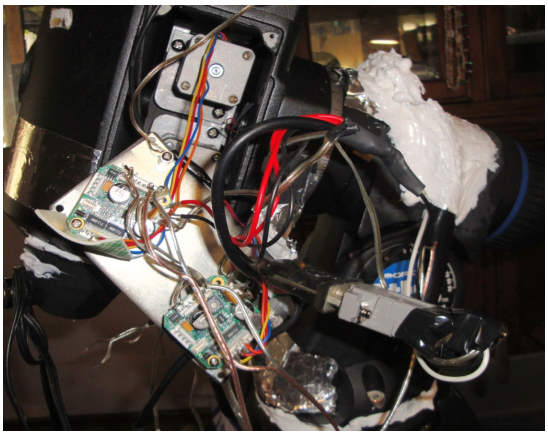

Figure 3. Mount stepper motor driver/controller modification.

The prototype 1 implementation (until summer 2011) performance was satisfactory except for pointing, due in part to the equatorial mount electronics and to the fact that our prototype 1 was mounted on the side wall of a wooden building. While the mount worked reliably, the electronics driving the stepper motors and the communication protocol to the electronics did not easily allow high performance tracking. This problem, combined with the fact that the mounting on a wooden wall did not provide a very stable reference, let to large drifts in pointing (approximately 1" to 5" per mn). This issue is addressed in our second prototype (in use since summer 2011) by:

- Mounting the unit on a sturdy metal frame, directly bolted to a ground concrete pad

- Replacing the native mount electronics with stepper controller+driver circuits offering more fine control of pointing and tracking (allowing for example small updates in tracking speed without introducing unwanted jumps/interruptions in the tracking)
- Implementing closed loop guiding: the images acquired are continuously used to refine pointing and tracking

The original mount electronics were replaced in July 2011 by two EZHR17EN EZstepper circuits (vendor: Allmotion) to improve tracking: the original circuit had unexplained behaviors and somewhat unreliable communication issues with the host computer. The EZstepper also provides more flexibility, and homing can be done without requiring the computer polling limit switch status.

4. DATA ACQUISITION SOFTWARE

4.1 Low level system architecture

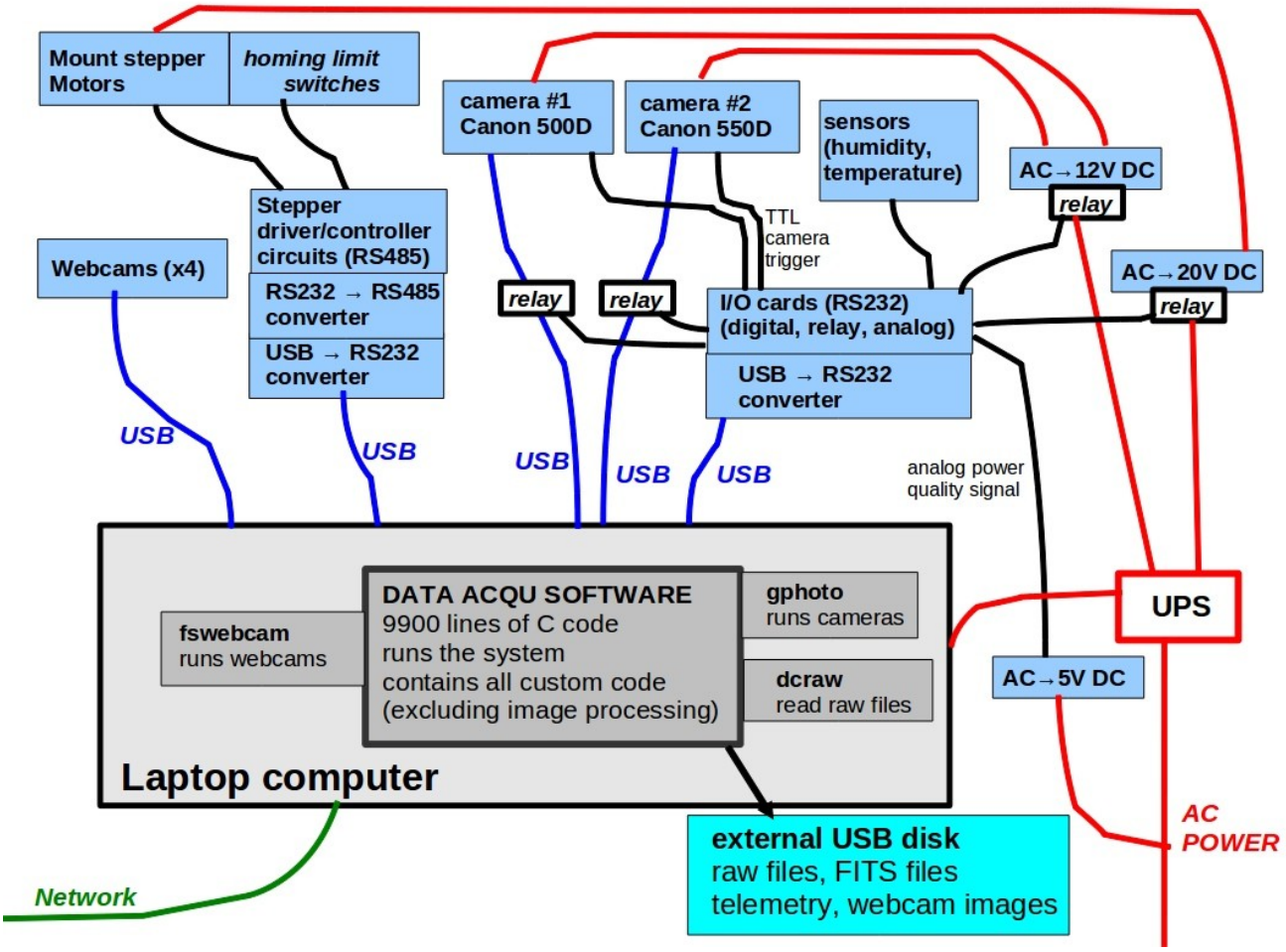

Figure 4. System architecture. A single laptop computer controls all hardware.

Figure 4 shows the overall system architecture. A single laptop computer controls all hardware. The cameras are linked to the computer by USB cables. When driven in USB mode, the gphoto software is used to acquire images and download them. The USB channel can also be de-activated (with a relay) to allow off-line camera control from a TTL trigger signal. This second mode of operation allows for higher duty cycle, but the images are then only available at the end of

the observation (morning), when they are downloaded from the camera memory card through the USB cable. The system makes extensive use of open source software for low-level control of the cameras and webcams: gphoto and dcraw are used to control the cameras and read RAW files, and fswebcam drives the webcams.

4.2 Scheduling

The data acquisition software monitors external sensors (humidity, temperature, light level coming from webcams) to decide if the system should be observing. An ASCII file contains priority fields (ranked) to be observed. If the file is empty or none of the fields is accessible (too low, or too close to the moon), a random pointing is chosen, and will be adopted for the next few exposures – after which a new random pointing will be chosen.

4.3 Astrometry

Each frame is referenced to an astrometric grid by comparison with the Hipparcos/Tycho catalog. The data acquisition software already provides a good estimate of the astrometic pointing, easing comparison with the catalog. The astrometric solution for each frame consists of 30 parameters: pointing (2 parameters), field rotation, plate scale and distortion coefficients to 4th order (26 parameters). Over the 10x15 deg field, agreement between the photocenters and catalog is within about a quarter of a pixel RMS, and likely dominated by pixelization effects (the photocenter is not an accurate estimate of the star location in the image).

5. PHOTOMETRY

5.1 Description photometric data reduction approach

Our photometric measurement is differential: other stars in the field are used to construct a reference against which the target star is compared. Choosing the optimal of PSF(s) used for comparison with the target star is essential to compensate for error terms correlated with other sources (variable extinction due to clouds and airmass, color effects, detector non-linearity). The choice of the comparison PSFs is therefore critical to achieving photometric precision, and is complicated by the detector's undersampling of the PSF, discussed in the next paragraph.

The main challenge to precision photometry with a low-cost DSLR-based system is to overcome errors due to PSF sampling, which are particularly serious in our system, as the pixel size is comparable to the PSF size, and the pixels are colored (25% of pixels are red-sensitive, 50% are green-sensitive and 25% are blue-sensitive). This issue could be mitigated by defocusing the image, thus spreading light of each star on many pixels. For example, defocusing star images to a 35 pixel diameter disk, a previous study[2] reports achieving 1% photometric accuracy in each of the 3 detector color channels over 90 sec exposures with a 203 mm telescope, and measuring transit depth to 0.1% (1 millimagnitude) for a 1hr duration transit. While this scheme is appropriate for photometry of a small number of bright stars, it is not suitable for a transit survey aimed at monitoring a large number of stars, as the combined loss of angular resolution (crowding limit) and faint-end sensitivity (mixing starlight with background) would have a large impact on the survey performance. In addition to the PSF sampling issue, a large number of variables can affect the measured apparent flux from stars (for example airmass, color extinction effects, PSF variations). Comparison PSF(s) used for differential photometry must be chosen to include these effects, either by choosing stars which are subjected to the same errors, or by understanding, modeling and compensating for these effects.

Our approach to solving these challenges relies on an image-based identification of suitable reference PSFs. The wide field image delivered by the system offer a large number of potential reference targets. We perform image cross-correlations between our target and other stars in the field to select PSFs which have the intensity distribution amount pixels as the target for each image of the sequence. **This step implicitly selects PSFs that have the same color, experience the same optical aberrations, fall on the same fractional pixel position and experience the same local detector defects as the target,** without having to compute explicitly these parameters. An optimal linear combination of selected candidate PSFs is then perform to construct a template against which the target images are compared to produce the photometric light curve. While similar schemes have previously been applied to lightcurves[8,9], the strong pixelization issues in our system require image-level processing before a lightcurve is created.

5.2 Example data

The scheme described in the previous section was implemented and used to produce a lightcurve for HD54743, observed on 2011-04-15 (UT). Thirty consecutive 65-sec exposures were acquired at ISO100. The images were acquired during bright time, with a relatively strong background (level = 2500 ADU, 2600 ADU and 1900 ADU per pixel per exposure in R, G and B respectively). This dataset is especially challenging for photometry, as the PSF is strongly undersampled (in part due to the fact that the camera's anti-aliasing filter has been removed), the detector is a color CMOS array, and the tracking is relatively poor, with a drift of approximately 5" per minute (0.5 pixel between consecutive frames). We note that the poor tracking was later solved by replacing the electronics in the mount, as detailed in section 3.2.

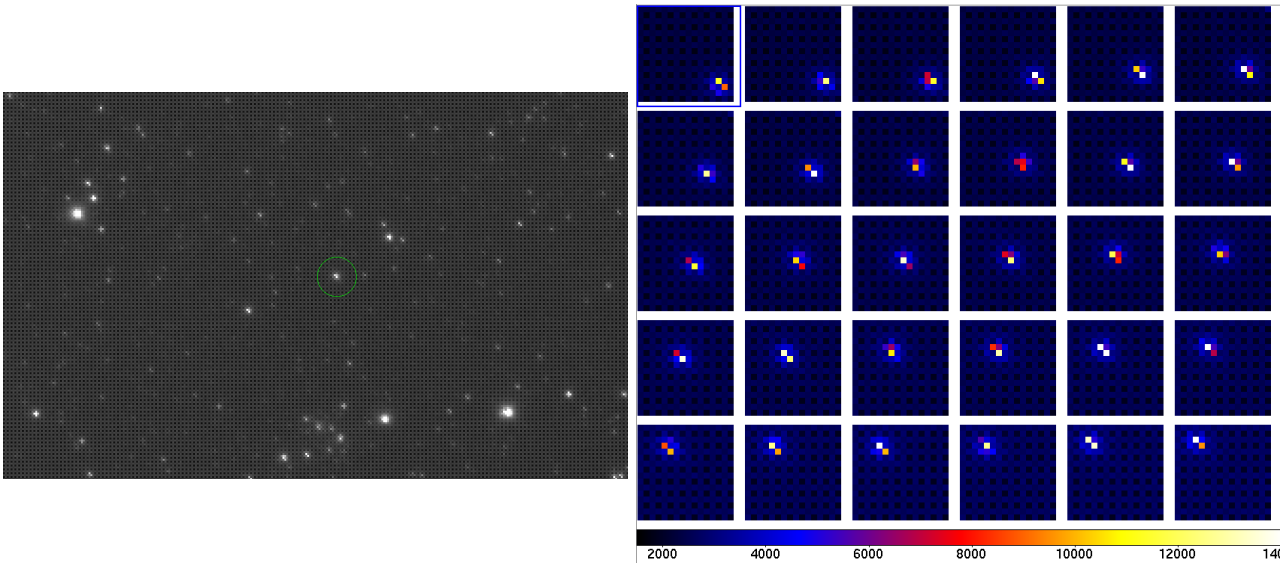

Figure 5. Left: Single frame (detail) showing star HD54743, circled. Right: Sequence of consecutive images of HD54743, showing the part of the detector where the star image is located.

Figure 5 shows that tracking errors move the star's image across different pixels, and that the combination of these tracking errors, the undersampling of the PSF by the detector and the fact that the detector is a color array, create a highly variable star image from frame to frame. Not surprisingly, the aperture photometry extracted from these frames is therefore a poor estimate of the actual star flux. Figure 6 (left) shows that aperture photometry leads to ~10% RMS variation in the measured flux from frame to frame. Our proposed algorithm reduces the error to about 2% per color channel.

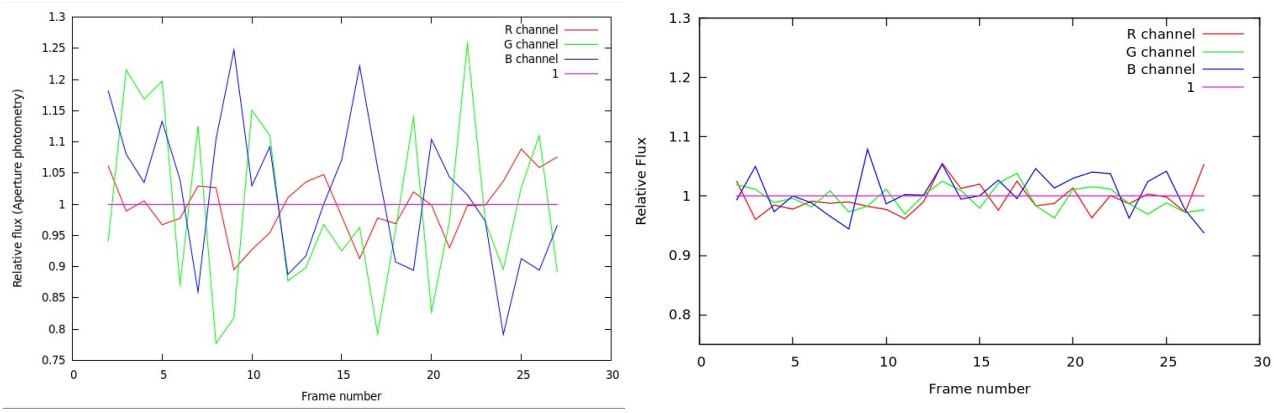

Figure 6. Photometry light curve with aperture photometry (left) and with our proposed data reduction scheme (right).

6. CONCLUSIONS

We have demonstrated that a relatively inexpensive robotic imaging system can be built and operated using mostly commercially available components. The total cost of our system is approximately $10k for an etendue of about 1 square degree square meter – significantly more affordable than hardware typically used for professional astronomy. The system has demonstrated reliability and fully robotic operation for more than a year, and can easily be duplicated.

A major challenge of using a color CMOS array for photometry is the pixelization of the undersampled PSF on the color matrix of pixels. Conventional aperture photometry is not suitable for these detectors, but an algorithm that carefully selects comparison PSFs using image-based correlations with the target star was successful at removing most of the pixelization errors. In fact, the 2% photometric accuracy over 1min reported in this paper approaches the photon noise limit and scintillation limit. When reaching these fundamental limits, the scientific merit of the system is purely measured by cost vs. etendue, and according to this metric, our proposed system is highly competitive. We therefore conclude that a particularly cost-effective strategy for exoplanet transit surveys would be to deploy a large number of units similar to the one described in this paper.

ACKNOWLEDGMENTS

This project was made possible thanks to Bo Reipurth and Josh Walawender of the Variable Young Stellar Object Survey (VYSOS) project, and the Mauna Loa observatory. Paul Stewart (University of Sydney) provided valuable help to install the system. Josh Walawender allowed the system to use VYSOS's weather monitoring and provided assistance in setting up the hardware at the site.

REFERENCES

[1] Fiacconi, D. and Tinelli, L., "Light curve analysis of XX Cygni from data taken using DSLR," Open European Journal on Variable Stars 114, 1–+ (2009).

[2] Littlefield, C., "Observing Exoplanet Transits with Digital SLR Cameras," Journal of the American Association of Variable Star Observers (JAAVSO) 38, 212–+ (2010).

[3] Hoot, J. E., "Photometry With DSLR Cameras," Society for Astronomical Sciences Annual Symposium 26, 67–+ (2007).

[4] Buil, C., "Spectroscopy, CCD and Astronomy," http://www.astrosurf.org/buil/ (2011).

[5] Clark, R. N., "Digital Camera Sensor Performance Summary," http://www.clarkvision.com (2011).

[6] Pokhvala, S. M., Zhilyaev, B. E., Reshetnyk, V. M., "High-speed multicolor photometry with CMOS cameras," Advances in Astronomy and Space Physics (2012)

[7] Walawender, J., Reipurth, B., and Paegert, M., "Computer Infrastructure for the Variable Young Stellar Objects Survey," Proceedings, Telescopes from Afar, (2011).

[8] Kov´cs, G., Bakos, G., and Noyes, R. W., "A trend filtering algorithm for wide-field variability surveys," MNRAS 356, 557–567 (2005).

[9] Tamuz, O., Mazeh, T., and Zucker, S., "Correcting systematic effects in a large set of photometric light curves," MNRAS 356, 1466–1470 (2005).